Threshold effects in strong-field detachment of H^- and F^-: Plateau enhancements and angular distribution variations

K. Krajewska,[1,2] Ilya I. Fabrikant,[1] and Anthony F. Starace[1]
[1]*Department of Physics and Astronomy, The University of Nebraska, Lincoln, Nebraska 68588-0111, USA*
[2]*Institute of Theoretical Physics, Warsaw University, Hoża 69, 00-681 Warszawa, Poland*
(Received 12 June 2006; published 8 November 2006)

Above-threshold detachment (ATD) rates for H^- and F^- ions in the high-energy plateau region are calculated as functions of photon number and laser intensity by solving the time-dependent Schrödinger equation within the Sturmian-Floquet approach. Pronounced enhancements of the ATD rates are found (up to an order of magnitude) as the laser-field intensity passes across ponderomotive-potential-induced channel closings. We confirm the zero-range potential model results of Borca *et al.* [Phys. Rev. Lett. **88**, 193001 (2002)] for negative ions whose initial states have *s* symmetry, and we investigate here the case of initial states having *p* symmetry. Depending on the symmetry of the initial state, the enhancement is found to be most pronounced for even- or odd-channel closures, which is consistent with threshold laws applicable at the closing of particular multiphoton channels. Variations of ATD electron angular distributions as functions of laser intensity near channel closings are also investigated and found to be sensitive to initial-state symmetry.

DOI: 10.1103/PhysRevA.74.053407 PACS number(s): 32.80.Rm, 32.80.Gc

I. INTRODUCTION

Atomic systems exhibit highly nonlinear responses to intense laser radiation, becoming ionized with absorption of many more photons than necessary to produce continuum electrons, a phenomenon known as above-threshold ionization (ATI) [1] (for reviews, see, e.g., [2–5]). One observes regularly spaced peaks (in intervals of the photon energy) in the energy spectrum of ejected electrons. The simplest and most intuitive description of the ATI energy spectrum is provided by the well-known "rescattering" or "three-step" semiclassical model [6,7]. In this picture, in which both the laser field and the ionized electron are treated classically, the so-called "direct" electrons are ionized without further interaction with the parent ion and have kinetic energies up to $2U_p$, where U_p is the ponderomotive energy, i.e., the energy of oscillation of an electron in the laser field. These direct electrons contribute to the low-energy part of the ATI spectrum, which comprises a sequence of electron peaks having decreasing intensities for increasing electron energy. The high-energy ATI spectrum, comprised of electron peaks ranging in energy up to $10U_p$ and having roughly comparable intensities (thus forming the characteristic "plateau"), is believed to originate from the rescattering of ionized electrons by the ionic core under the influence of the driving laser field, subsequent to which the rescattered electrons are further accelerated by the laser field.

Although the cutoff energy of the "hot" electrons comprising the plateau of the high-energy ATI spectrum is well described by the classical analysis, more detailed properties of the spectrum, such as the resonant-like enhancements that have been reported in experiments performed for rare gases [8–13], require a quantum treatment. Those measurements have shown that the envelope of the rescattering plateau does not remain flat, but instead exhibits resonant-like enhancements (as a function of the intensity of the driving laser field) of only a certain energy range of ATI electron peaks. At certain intensities, a small variation of the field strength raises a portion of the rescattering plateau by up to an order of magnitude. Such highly intensity-selective enhancements in the yield of hot electrons, together with a detailed structure of the ATI peaks (composed of three narrow subpeaks each), have been observed for xenon [8] and have been found to be even more pronounced in experiments for argon [9,10]. This experimental evidence for a resonance-like scenario being involved in high-energy above-threshold ionization was confirmed also by more recent experiments [11–13] for various rare-gas atoms.

At present, the precise origin of the resonant-like enhancements of ATI plateau electrons remains a subject of theoretical discussion and differing interpretations [10–12,14–20]. One explanation posits the idea of multiphoton resonances between the ponderomotively upshifted Rydberg states and the ground state of an atom as being crucial for the enhancement [10,11,14,15,19,20]. In Refs. [10,11,14,15], this concept arose when the single-active-electron (SAE) approximation [21] using a model potential for the e-Ar^+ interaction was used to solve numerically the time-dependent Schrödinger equation. The results of these one-electron calculations modeled the observed ATI spectra very well, including even very subtle ATI peak substructures. These calculations thus showed that ATI plateau resonance features cannot be due to multielectron resonances, but, it was proposed instead, to single-electron Rydberg resonances in the laser field. The same method applied to a one-dimensional soft-Coulomb potential [19,20] supported this hypothesis. In Refs. [19,20], simulations using a one-dimensional zero-range potential (ZRP) were also performed. Despite the fact that the zero-range potential supports only a single bound state, however, similar enhancements were observed in the calculated above-threshold detachment (ATD) spectra. It was suggested that for model potentials that do not have a Coulomb tail, certain light-induced states [22] take over the role of Rydberg states, so that the plateau enhancements in the case of short-range potentials have a similar origin.

There are some ambiguities regarding these interpretations of resonance-like enhancements of ATI plateaus as arising from either ponderomotively upshifted Rydberg state resonances or light-induced-state resonances. One is that Rydberg states are very short-lived, i.e., they are easily ionized in an intense laser field. Thus there is a question of whether such short-lived states can influence the ATI spectra and, in particular, whether they can cause the enhancement of the high-energy ATI plateau. Another is that for the case of short-range potentials, the idea of attributing the enhancements to light-induced resonance states is based on one-dimensional calculations [19,20]. However, for the case of a three-dimensional short-range potential in the presence of a strong laser field, light-induced states have not been found to exist [23]. Yet another ambiguity is that if the enhancements originate from a multiphoton resonance with an intermediate state, then one would expect the entire ATD spectrum at higher energies to be enhanced; however, only a range of ATD peaks at the lower- to mid-energy region of the plateau are observed to be enhanced.

An alternative explanation relates the resonant-like enhancements of ATI and ATD plateaus to laser-intensity-induced multiphoton channel closings (CCs) [12,16–18], i.e., to a threshold-related effect. Because the ponderomotive potential raises the continuum threshold, the minimum number of photons necessary to ionize an electron from an atom (or detach an electron from a negative ion), n, increases with increasing laser intensity, or, in other words, the n-photon channel for ionization or detachment can become closed as the laser intensity increases. Near the intensity for which this happens, a group of ATI (or ATD) peaks within the rescattering plateau is raised significantly. In the context of CCs, the enhancement has been interpreted as either a consequence of constructive interference between different "quantum trajectories" that takes place at intensities near the channel closings [12,16,18] or as an example of well-known quantum-mechanical threshold laws applicable at the closing of multiphoton channels [17]. Both those pictures call into question the role of Rydberg or excited states as being essential for the enhancement, since in relevant numerical simulations that exhibited the intensity-induced plateau enhancements [12,16–18], a three-dimensional zero-range potential model (in which there are no excited states) was used.

Although the experiments with argon reported in Ref. [12] were simulated by ZRP model calculations and qualitatively good agreement with theory was found, the model itself is more suitable for the description of ATD processes, which is the main subject of this paper. In contrast to the ZRP models that have been used so far to analyze the enhancement of ATD plateau spectra [12,16–18], we employ here finite range model potentials to describe the negative ions we treat and to analyze high-energy above-threshold detachment. The key question that we address is how the symmetry of the negative-ion initial state affects the laser-induced enhancement of the rescattering plateau. The ZRP model has only one bound state of s symmetry. In this paper, we compare and contrast the role of the initial-state electron's orbital angular momentum symmetry on the laser-induced enhancements of the ATD plateau spectra. We also explore the role of this symmetry on the angular distributions of ATD electrons in the vicinity of CCs. Our results for finite-range model potentials that do not have excited states (above the state of the valence electron) confirm the ATD plateau enhancements we obtain as due to ponderomotive potential-induced channel closings with the largest enhancements corresponding to the closing of even or odd multiphoton channels in the cases of initial s- or p-electron symmetries, respectively. They may thus be regarded as dramatic manifestations of well-known threshold anomalies of collision theory [24–29] for the case of multiphoton processes. (A brief report of these findings has been given elsewhere [30].) We find also that the ATD electron angular distributions are sensitive to the initial-state symmetry of the active electron and to whether an even or odd number of photons are absorbed.

This paper is organized as follows. A rigorous treatment of ATD within the Floquet-Sturmian theory framework is given in Sec. II. In Sec. III, we introduce the model potentials representing the negative ions that we consider, whereas in Sec. IV the threshold behavior of multiphoton detachment at channel closings is demonstrated. Finally, in Secs. V and VI, numerical results for the partial rates and angular distributions of ionized electrons as functions of changing laser-field intensity are discussed. We summarize our results and discuss our conclusions in Sec. VII. In the Appendix, we discuss the normalization of results for many-electron systems treated by means of the SAE approach. Note that throughout this paper we use atomic units unless otherwise noted.

II. MULTIPHOTON DETACHMENT PROBABILITIES VIA FLOQUET STATES

For decaying processes (e.g., ionization or detachment), the initial state of a quantum system, $|\psi_0(t)\rangle = e^{-iE_0 t}|\psi_0\rangle$, in the presence of a time-periodic strong laser field can be represented within the Floquet theory (for a review, see Ref. [31]) in the quasistationary form

$$|\psi(t)\rangle = e^{-iEt}|\phi_E(t)\rangle, \tag{1}$$

where E is the quasienergy, and the Floquet, or quasienergy, state $|\phi_E(t)\rangle$ is periodic in time, with the same period as the laser field. In this case, the quasienergy is complex,

$$E = E_0 + \Delta - i\frac{\Gamma}{2}, \tag{2}$$

where Δ describes the ac Stark shift of the initial-state energy level and the imaginary part is simply related to the total decay rate, Γ, of the system. The quasienergy E and the associated state $|\phi_E(t)\rangle$ are determined by solving the eigenvalue (Floquet) equation,

$$\left(H_0 + V(t) - i\frac{d}{dt}\right)|\phi_E(t)\rangle = E|\phi_E(t)\rangle, \tag{3}$$

with complex boundary conditions imposed on the decaying states in external fields. Here H_0 represents the system's field-free Hamiltonian, whereas the interaction of the system with the external field is described by the potential $V(t)$.

We consider detachment of a negative ion by a linearly polarized laser field having frequency ω and its polarization

vector directed along the z axis, $\hat{\boldsymbol{\varepsilon}}=\hat{\boldsymbol{z}}$. The electric field and the vector potential are $\boldsymbol{\mathcal{F}}=\mathcal{F}_0\hat{\boldsymbol{\varepsilon}}\cos\omega t$ and $\boldsymbol{\mathcal{A}}=\mathcal{A}_0\hat{\boldsymbol{\varepsilon}}\sin\omega t$, respectively, where $\mathcal{A}_0=-c\mathcal{F}_0/\omega$, and $\mathcal{F}_0$ describes the strength of the laser field. We treat the ion within the SAE approximation, with the electron-atom interaction described by a short-range potential W. The atomic Hamiltonian of the system is, therefore,

$$H_0=\frac{\boldsymbol{p}^2}{2\mu}+W, \tag{4}$$

and the electron-laser field interaction in the dipole velocity gauge (which is used throughout this work) is

$$V(t)=\frac{1}{\mu c}\boldsymbol{\mathcal{A}}(t)\cdot\boldsymbol{p}, \tag{5}$$

where μ is the electron's reduced mass and $\boldsymbol{p}$ is its canonical momentum. The Fourier expansion of the Floquet state $|\phi_E(t)\rangle$,

$$|\phi_E(t)\rangle=\sum_n e^{-in\omega t}|\phi_E^{(n)}\rangle, \tag{6}$$

substituted into Eq. (3), results in the following system of time-independent coupled equations for the harmonic components $|\phi_E^{(n)}\rangle$:

$$(E+n\omega-U_p-H_0)|\phi_E^{(n)}\rangle=V_+|\phi_E^{(n-1)}\rangle+V_-|\phi_E^{(n+1)}\rangle, \tag{7}$$

where the ponderomotive energy of the electron quiver motion is $U_p=\mathcal{F}_0^2/4\mu\omega^2$, and where V_+ and V_- are defined as the Fourier coefficients of the potential $V(t)$,

$$V_+e^{-i\omega t}+V_-e^{i\omega t}=V(t). \tag{8}$$

The harmonic component $|\phi_E^{(n)}\rangle$ in the series expansion in Eq. (6) describes an electron that has absorbed a net energy of $n\omega$. At large distances from the atomic core, the electron that has been detached with absorption of n photons is described by a spherical wave,

$$|\phi_E^{(n)}\rangle\sim\frac{e^{ik_nr}}{r}, \tag{9}$$

where k_n stands for the wave number, which depends on the quasienergy E,

$$k_n=\sqrt{2\mu(E+n\omega-U_p)}. \tag{10}$$

For open channels, spherical waves, like the one in Eq. (9), should be outgoing waves, so that $\mathrm{Re}\,k_n>0$. This requirement is fulfilled for channels for which the number of absorbed photons $n\geqslant n_0$, with n_0 being the minimum number of photons necessary to detach the electron. In other words, for open channels we have $\mathrm{Re}\,E+n\omega-U_p>0$. On the contrary, channels with $n<n_0$ (or, equivalently, channels for which the inequality $\mathrm{Re}\,E+n\omega-U_p<0$ holds) are closed, since in this case $\mathrm{Im}\,k_n>0$, so that Eq. (9) represents an exponentially damped wave. In actual computations [32], the infinite system of coupled equations (7) is solved only after truncation at some point. Then, the truncated system of equations is solved by expanding each harmonic component $\phi_E^{(n)}(\boldsymbol{r})$ in terms a basis set of complex radial Sturmian functions $S_{Nl}^{(\kappa)}(r)$ and spherical harmonics $Y_{lm}(\hat{\boldsymbol{r}})$,

$$\phi_E^{(n)}(\boldsymbol{r})=\sum_{Nlm}c_{Nlm}^{(n)}\frac{S_{Nl}^{(\kappa)}(r)}{r}Y_{lm}(\hat{\boldsymbol{r}}), \tag{11}$$

where

$$S_{Nl}^{(\kappa)}(r)=\frac{1}{(2l+1)!}\sqrt{\frac{-i\kappa(N+2l)!}{(N+l)(N-l)!}}(-2i\kappa r)^{l+1}\times e^{i\kappa r}{}_1F_1(1-N;2l+2;-2i\kappa r), \tag{12}$$

where ${}_1F_1(n;l;z)$ is the confluent hypergeometric function [33]. Here, κ stands for the complex parameter of the basis, which, in order to obtain solutions of physical significance (i.e., satisfying the appropriate complex boundary conditions), has to be chosen such that

$$|\arg(\kappa)-\arg(k_n)|<\frac{\pi}{2} \tag{13}$$

for all wave numbers k_n [32]. Finally, by projecting Eq. (7) onto the Sturmian basis and by making use of the orthonormality relation,

$$\int_0^\infty dr S_{nl}^{(\kappa)}(r)\frac{1}{r}S_{n'l}^{(\kappa)}(r)=\delta_{nn'}, \tag{14}$$

one arrives at a matrix equation for the coefficients $c_{Nlm}^{(n)}$. This enables one to find the quasienergies and the associated Floquet states by solving the resulting non-Hermitian matrix eigenvalue problem. For details of numerical methods used in this context, see Ref. [32].

The theoretical formulation of the detachment probability rates is given in great detail elsewhere [31,34–37]. Here, we summarize only the main formulas employed in our calculations. Sufficiently far from the atomic potential W, after absorbing $n\geqslant n_0$ photons, a detached electron having positive energy $E_f=k_f^2/2\mu$ moves in the laser field with the drift momentum $\boldsymbol{k}_f$, where

$$k_f=\sqrt{2\mu(\mathrm{Re}\,E+n\omega-U_p)}. \tag{15}$$

The differential rate $d\Gamma^{(n)}/d\Omega$ for n-photon detachment when the electron emerges into the solid angle $d\Omega$ along the direction of the vector $\boldsymbol{k}_f$ is

$$\frac{1}{2\pi}\frac{d\Gamma^{(n)}}{d\Omega}=\mu k_f|M_n(\boldsymbol{k}_f)|^2, \tag{16}$$

where $M_n(\boldsymbol{k}_f)$ is the n-photon detachment amplitude. This transition amplitude can be expressed in terms of Bessel functions $J_n(z)$ [31,34–37],

$$M_n(\boldsymbol{k}_f)=\sum_N e^{i(N-n)\beta}J_{N-n}(-\alpha)\langle\boldsymbol{k}_f|W|\phi_E^{(N)}\rangle, \tag{17}$$

where α and β are real, and are defined by

$$\alpha \cos(\omega t - \beta) = \frac{1}{\mu} \int^{t} d\tau \boldsymbol{k}_f \cdot \boldsymbol{\mathcal{A}}(\tau). \tag{18}$$

The partial rate $\Gamma^{(n)}$ for detachment into a specific channel n can be obtained from Eq. (16) by averaging over all possible directions of the ejected electron,

$$\Gamma^{(n)} = \int \frac{d\Gamma^{(n)}}{d\Omega} d\hat{\boldsymbol{k}}_f. \tag{19}$$

At this point, it is important to note that the sum of all possible partial rates $\Gamma^{(n)}$, starting from $n=n_0$, should result in the total detachment rate Γ. On the other hand, as follows from the definition of the quasienergy E, Eq. (2), we have $\Gamma=-2$ Im E. We arrive, therefore, at the following condition:

$$\sum_{n \geq n_0} \Gamma^{(n)} = -2 \text{ Im } E, \tag{20}$$

which provides a test for the validity of the approach being used, which we have monitored closely during our computations.

III. SINGLE-ACTIVE-ELECTRON APPROXIMATION

Our considerations so far have been general in the sense that they have accounted for any ionic system that has only one outer electron. To be more specific, let us introduce here model potentials for the negative ions of hydrogen, H^-, and fluorine, F^-. Within the framework of the SAE approximation, the active electron in both ions may be described as moving in an atomic potential W of Yukawa type,

$$W(r) = -W_0 \frac{e^{-\lambda r}}{r}. \tag{21}$$

The potential parameters, $W_0>0$ and $\lambda>0$, are fitted for each ion separately, as discussed in the next subsections. Note that the question of the normalization of detachment rates for many-electron ions that are treated in the single-active-electron approximation is discussed in the Appendix. Note also that from this point on in this paper we assume $\mu=1$ [cf. Eq. (4)] unless indicated otherwise.

A. Negative hydrogen ion

For the negative hydrogen ion, H^-, we make use of the model potential introduced in Ref. [34] and reconsidered later by the authors of Ref. [37]. It has the Yukawa form (21), with the parameter values $W_0=1.1$ a.u. and $\lambda=1.0$ a.u. For these values of W_0 and λ, the potential $W(r)$ supports only one bound state (the $1s$ state, with orbital angular momentum $l=0$) having a binding energy $-0.027\,565\,4$ a.u., which is very close to the experimental value [38]. The model potential ground-state wave function reproduces also the radial charge distribution given by an accurate two-electron probability density integrated over the spatial coordinates of one of the electrons [34]. For the case of a CO_2 laser, operating at the frequency $\omega=0.0043$ a.u. ($\lambda=10.6$ μm), for small intensities of the laser field we find that detachment of H^- requires the absorption of at least seven photons. This threshold for photodetachment increases when the laser-field intensity is increased. For completeness, we note that all intermediate states accompanied by emission of up to a maximum of seven photons and absorption of up to 65 photons have been taken into account in our calculations; this particular choice of processes that are included in our calculations gives reliable, convergent results.

B. Negative fluorine ion

The negative fluorine ion, F^-, is modeled by the Yukawa potential (21) with parameter values $W_0=5.0745$ a.u. and $\lambda=1.0$ a.u. As for the case of H^-, our choice for λ accounts for screening of the nuclear charge by the atomic charge cloud of inner electrons, and the potential strength W_0 is adjusted to reproduce the correct binding energy of the ion. The main difference between these two cases lies in the symmetry of the initial bound (valence) state, which for F^- has p-state symmetry. In the present model, the $2p$ state has an energy of $-0.124\,98$ a.u. (while the experimental value is $-0.124\,99$ a.u. [39]); there exist also the $2s$ state with the energy -0.3292 a.u. and the $1s$ ground state, which is located significantly lower in energy.

In order to investigate accurately the enhancement of the ATD plateau, we must be concerned in our model with multiphoton resonances involving the bound p state. We note that when our model F^- ion is exposed to a laser field with frequency $\omega=0.0253$ a.u., which corresponds to the wavelength 1.8 μm, as in the experiment of Ref. [40] and in the theoretical work of Refs. [41–43], then in the weak-field limit a minimum of five photons is required to detach the $2p$ electron, while at least nine photons are needed to have a $2p-2s$ resonance. To check on the role of multiphoton resonances in the enhancement of the high-energy ATD spectrum resulting from detachment of the valence $2p$ electron, we have performed numerical calculations for two cases: (a) when detachment is realized through intermediate states involving the emission of up to eight photons (the nonresonant case), and (b) when detachment is realized through intermediate states involving the emission of up to 15 photons (the resonant case). In both cases, the maximum number of absorbed photons is 70. Remarkably, in the range of the laser-field intensity that we have investigated, we have not found any discrepancies between the calculated results for these two cases.

IV. THRESHOLD BEHAVIOR OF MULTIPHOTON DETACHMENT AT CHANNEL CLOSINGS

Before presenting our numerical results, we review briefly the theory of threshold behaviors near channel closings. Analysis of the threshold behavior of multiphoton detachment by standard collision methods is complicated by the fact that photons have special properties as compared to particles. These properties include the nonlocal character of photons in coordinate space, "which prevents their description by orthodox spatial wavefunctions" ([25], p. 336).

If one wishes to remain within the framework of a stationary approach to the problem, there are two ways out of this

difficulty. The first is to consider the Floquet equation for the quasienergy (3) and to look for the imaginary part of the quasienergy describing the partial width for $(N+s)$-photon detachment near the N-photon threshold $(s=1,2,\ldots)$. This approach, although mathematically rigorous, contains all the difficulties related to finding the correct complex solutions of the Floquet equation (see Sec. II).

A second approach, which will be developed below, is more physically transparent, although less rigorous mathematically. It is similar to the truncated-threshold approximation used by Potvliege and Shakeshaft [35]. Instead of the explicit introduction of the initial state (for a bound electron in the presence of a laser field), we introduce instead a source term that is responsible for outgoing flux in the open (detached electron) channels. The point here is that the initial state is closed with respect to the electron energy. Although it is open with respect to the photon energy, and could be considered as a bound electron plus N photons, it cannot be described by the standard theory of threshold behavior, since photons cannot be described by a wave function in position space.

Thus, the multicomponent Floquet wave function $\phi_E(\boldsymbol{r})$ satisfies the set of equations (7),

$$(H_0 - E - n\omega + U_p)\phi_E^{(n)} + V_+\phi_E^{(n-1)} + V_-\phi_E^{(n+1)} = S_n. \tag{22}$$

In order to investigate the threshold behavior of photodetachment, the acceleration gauge is more appropriate. $S_n(\boldsymbol{r})$ is the source term responsible for the coupling with the initial state. In the simplest case of one-photon detachment, $S_1 = V_+\phi_E^{(0)}$, where $\phi_E^{(0)}$ is the electron wave function of the initial state. The major assumption here is that $\phi_E^{(0)}$ is not affected by the back coupling $V_-\phi_E^{(1)}$; therefore, $\phi_E^{(0)}$ can be treated as a stationary state, and the energy of the system is real. This assumption is realistic unless the field is superstrong, in which case the discussion of threshold phenomena becomes meaningless.

Let us consider now $N+1$ electronic channels with energies $E+n\omega-U_p$, $n=0,1,\ldots,N$. In the spirit of the R-matrix theory [25], we divide the whole space into two regions, inside and outside a sphere of radius a. We assume that for $r>a$, all electromagnetic coupling between channels vanishes. This can be done in the acceleration gauge if $a>\alpha_0$ [44], where $\alpha_0=\mathcal{F}_0/\mu\omega^2$ is the amplitude of the electron quiver motion. Obviously, with the growth of $\mathcal{F}_0$ or decrease of ω, the radius a should be increased, and this makes the energy range over which the threshold law holds very limited.

Inside the R-matrix sphere, the solution of the system (22) can be written in the following form:

$$\phi_E^{\text{in}}(\boldsymbol{r}) = f(\boldsymbol{r}) + u(\boldsymbol{r})A, \tag{23}$$

where ϕ_E^{in} is the solution vector with components $\phi_E^{(n)}, n=0,1,\ldots,N$, u is the general solution matrix of the *homogeneous* equations (without the source terms), with rows corresponding to different channels and columns corresponding to different linearly independent solutions, A is a vector of arbitrary coefficients, whereas f is a column corresponding to a particular solution of the *inhomogeneous* equations (22). Both f and u are determined by boundary conditions at the origin that are independent of energy; therefore, they can be considered as analytic functions of E. Outside the sphere, we have only outgoing waves in open channels, and exponentially decaying solutions in closed channels, so that the solution vector is

$$\phi_E^{\text{out}}(\boldsymbol{r}) = OT, \tag{24}$$

where O is the diagonal matrix of outgoing solutions having the asymptotic form

$$O_n \sim \exp\{i(k_n r - l\pi/2)\}/\sqrt{v_n}, \tag{25}$$

where k_n is the wave number in channel n [cf. Eq. (10)] and v_n is the electron velocity in channel n ($k_n=v_n$ in a.u.). The normalization of the solution O_n corresponds to unit flux density in the outgoing channel. Note also that for the case of ionization, the asymptotic phase of O_n should include the Coulomb phase. T in Eq. (24) is a vector of ionization amplitudes that determines the n-photon ionization rate. Specifically, the differential partial ionization rate dw_n in the direction $\hat{\boldsymbol{r}}$ is given by

$$dw_n = |T_n|^2 |Y_{lm}(\hat{\boldsymbol{r}})|^2 d\hat{\boldsymbol{r}}, \tag{26}$$

where l and m are the electron angular momentum and its projection in channel n. Writing now the matching equations for ϕ_E and its derivative and solving them for T, we obtain

$$T = (LO)^{-1}\,(Lf)|_{r=a}, \tag{27}$$

where

$$L = R\frac{d}{dr} - 1, \quad R = u\left(\frac{du}{dr}\right)^{-1}\Bigg|_{r=a}. \tag{28}$$

The equation for R corresponds to the standard definition of the R matrix [25].

In order to investigate the threshold behavior, we should express the analytical properties of O_n as a function of the channel energy $k_n^2=2(E+n\omega-U_p)$ explicitly. In the case of photodetachment, in which there are no long-range interactions outside the R-matrix sphere, O_n can be expressed as a linear combination of spherical Bessel and Neumann functions. Consequently, we can write

$$O = \xi(k^2)k^{-l-1/2} + i\,\eta(k^2)k^{l+1/2}, \tag{29}$$

where ξ and η are real entire functions of k^2, and k and l are diagonal matrices of linear and angular momenta. Substituting Eq. (29) into Eq. (27), we obtain

$$T = k^{l+1/2}(M - ik^{2l+1})^{-1}g, \tag{30}$$

where

$$M = -\,(L\eta)^{-1}\,(L\xi)|_{r=a}, \quad g = -\,(L\eta)^{-1}\,(Lf)|_{r=a}. \tag{31}$$

Equation (30) is an analog of an equation of Ross and Shaw [26]. The latter was obtained for collision channels not involving photons. Both the matrix M and the vector g are meromorphic functions of energy, E. For the purpose of investigating the threshold behavior, they are treated as ana-

lytical functions of energy, assuming no poles lie near the threshold.

Consider now the threshold behavior of the N-photon and the $(N+m)$-photon detachment processes near the threshold for N-photon detachment. This means that $|E+N\omega-U_p|$ is small, and $k_N^2=2(E+N\omega-U_p)$ can be both negative and positive. Let us call the N-photon channel number 1 and the $(N+m)$-photon channel number 2 and assume for simplicity that all other channels are taken care of by the source terms S_1 and S_2, or the corresponding terms g_1 and g_2 in Eq. (30). For $k_1^2>0$, both channels are open, and we have

$$T_i = s_i \frac{M_{jj}g_i - M_{12}g_i - is_j g_i}{(\det M)^2 - is_j M_{ii} - is_i M_{jj} - s_1 s_2}, \tag{32}$$

where $s_i=k_i^{2l_i+1}$, $i=1,2$; $j=2$ if $i=1$ and $j=1$ if $i=2$; and $\det M=M_{11}M_{22}-M_{12}^2$. The most interesting case is $l_1=0$, or $s_1=k_1$. For the detachment rate in channel 1, we obtain, in accordance with the Wigner threshold law ($|T_1|^2 \propto k_1$),

$$|T_1|^2 = k_1\left(\frac{c_1}{a+bk_1} + O(k_1^2)\right), \tag{33}$$

where

$$c_1 = (M_{22}g_1 - M_{12}g_1)^2 + (s_2 g_1)^2,$$

$$a = (\det M)^2 + (s_2 M_{11})^2, \quad b = 2M_{12}^2 s_2 \tag{34}$$

are all positive constants. For the threshold behavior in channel 2 [$(N+m)$-photon channel],

$$|T_2|^2 = s_2\left(\frac{c_2}{a+bk_1} + O(k_1^2)\right), \tag{35}$$

where $c_2=(M_{11}g_2-M_{12}g_1)^2$. Below the N-photon threshold, we have $k_1^2<0$. Defining $k_1=i\kappa$, we obtain

$$|T_2|^2 = s_2\left(\frac{c_1+\alpha\kappa}{a+\beta\kappa} + O(\kappa^2)\right), \tag{36}$$

where

$$\alpha = 2g_2(M_{11}g_2 - M_{12}g_1), \quad \beta = 2(M_{22}\det M + s_2^2 M_{11}). \tag{37}$$

Note that the signs of α and β, in contrast to b, are not defined, therefore we obtain two types of Baz' cusps [24]: (i) "up-down" and (ii) "down-down." In any event, the rate in the "old" [$(N+m)$-photon] channel is always dropping above the threshold of the "new" (N-photon) channel. In practice, this threshold behavior can be observed by increasing the light intensity. In this case, because the ponderomotive shift is increasing, k_1^2 is decreasing, and this leads to the growth of the $(N+m)$-photon detachment rate. However, this particular result has limited significance since we have used a two-channel approximation and assumed that channel 1 is s-wave dominated. Generally, one observes all four types of Baz' cusps [24], as we shall see in the next section.

V. HIGH-ENERGY ABOVE-THRESHOLD DETACHMENT

In order to judge the accuracy and convergence of our approach, we begin our analysis by comparing some of our results for multiphoton detachment rates for H^- with the available published results of Telnov and Chu [45] and of Gribakin and Kuchiev [46]. According to our arguments regarding the proper normalization of the initial-state wave function (presented in the Appendix), we readjust our results obtained with the Yukawa potential by multiplying them by the factor $(B/B_{\text{Yukawa}})^2=1.731$, where B is the exact asymptotic coefficient and B_{Yukawa} is the asymptotic coefficient resulting from the Yukawa potential. The results of Gribakin and Kuchiev should correspondingly be renormalized by multiplying them by the factor $(B/B_{\text{Gribakin}})^2/2=1.104$, where the additional factor $1/2$ rescales the cross section back to those appropriate for a single-active-electron model, as discussed in the Appendix. As one can see in Fig. 1, the agreement between the resulting three calculations is excellent (i.e., within $\leqslant 10\%$) for $n\leqslant 11$ for the laser-field intensity $I=1\times10^{10}\ \frac{\text{W}}{\text{cm}^2}$. For this laser intensity and $12\leqslant n\leqslant 22$, our results (which are lower) and those of Telnov and Chu [45] agree to within $\leqslant 17\%$, while for $23\leqslant n\leqslant 30$ the results of Ref. [45] decrease at a slower rate than ours, most likely owing to the different potentials used. (We note that this high n region lies beyond the cutoff of the ATI plateau for this intensity, $n=17$, and hence is far from the main focus of this paper.) For $n=12,13$ (i.e., at the onset of the plateau), the results of Gribakin and Kuchiev [46] are substantially lower than ours (as well as those of Ref. [45]), presumably owing to their omission of rescattering in their calculations. For a higher laser intensity, $I=3\times10^{10}\ \frac{\text{W}}{\text{cm}^2}$, Fig. 1 shows that the agreement between our results and the results of Ref. [45] is within $\leqslant 13\%$ over the entire range of n shown, as the influence of the atomic potential on the final results becomes smaller for this more intense laser field.

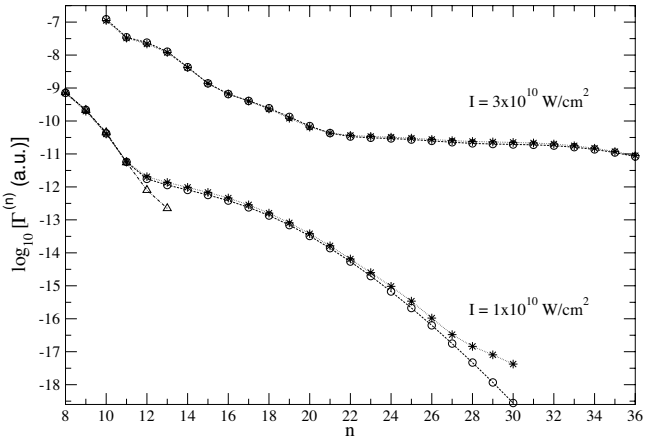

FIG. 1. Partial rates $\Gamma^{(n)}$ (in atomic units) for n-photon above-threshold detachment of H^- by a linearly polarized CO_2 laser field. The present renormalized results (open circles) are compared to the available published results of Telnov and Chu [45] (asterisks) for two laser intensities and to the available published (and renormalized) results of Gribakin and Kuchiev [46] (open triangles) for one laser intensity, as indicated in the figure. See text for details of the renormalization procedure.

We analyze next the ATD spectra as a function of laser intensity for the negative H^- and F^- ions irradiated by linearly polarized laser fields with frequencies $\omega=0.0043$ and

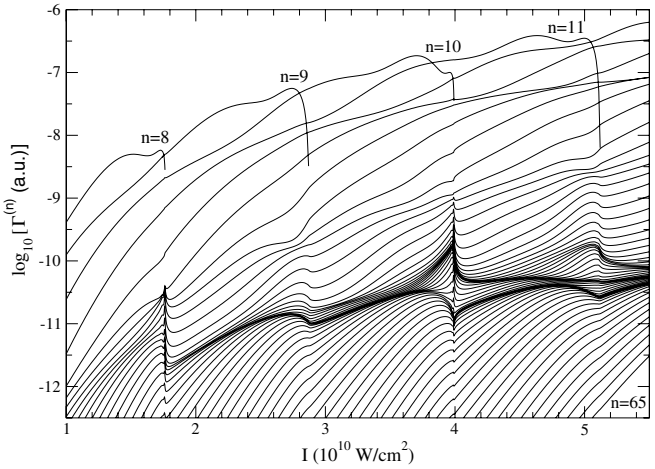

FIG. 2. Intensity dependence of the partial rates $\Gamma^{(n)}(I)$ for detachment of the H^- ion by a laser field operating at frequency $\omega=0.0043$ a.u., in the region where the ponderomotive shift causes the $n=8$, 9, 10, and 11 channel closures (at intensities 1.76, 2.87, 3.99, and 5.12×10^{10} $\frac{\mathrm{W}}{\mathrm{cm}^2}$, respectively). These results compare well with results of a ZRP model calculation [17].

0.0253 a.u., respectively. In Figs. 2 and 3, we present the respective partial rates $\Gamma^{(n)}$, in a.u., as functions of the laser-field intensity $I=(c/8\pi)\mathcal{F}_0^2$, given in units of $\frac{\mathrm{W}}{\mathrm{cm}^2}$ (using the conversion factor 1 a.u.$=6.436\,41\times10^{15}$ $\frac{\mathrm{W}}{\mathrm{cm}^2}$). In Fig. 2, we show the n-photon detachment rates for the H^- ion, $\Gamma^{(n)}$, for $8\leqslant n\leqslant 65$ and for a range of laser-field intensities such that the $n=8$, 9, 10, and 11 multiphoton detachment channels become closed. These results extend those of [17] (in which the ZRP model was used) to the case of a finite-range potential, and we find very good agreement with those previous results. For comparison, we note that in Ref. [17] the $n=8$, 9, and 10 channels become closed at the intensities $I=1.72$, 2.83, and 3.92×10^{10} $\frac{\mathrm{W}}{\mathrm{cm}^2}$, whereas in our case these closures

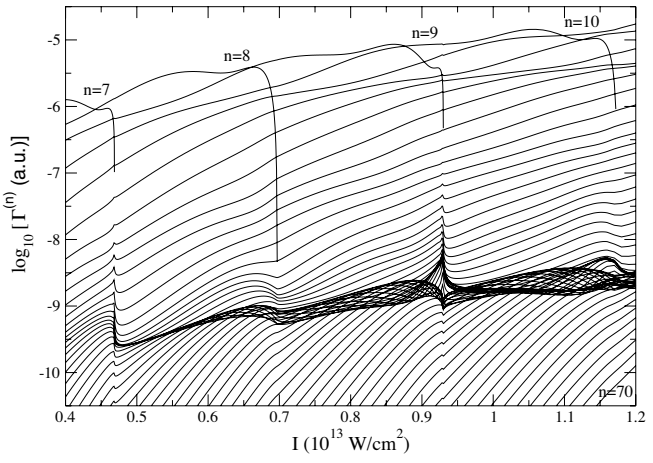

FIG. 3. The same as Fig. 2 but for the F^- ion irradiated by a laser field of frequency $\omega=0.0253$ a.u., in the region of intensities over which the $n=7$, 8, 9, and 10 channels become closed (at intensities of the laser field equal to 4.69, 6.97, 9.30, and 11.72×10^{12} $\frac{\mathrm{W}}{\mathrm{cm}^2}$, respectively). The results for the partial rates have been averaged over the projections of the initial angular momentum, $l=1$.

occur for intensities $I=1.76$, 2.87, and 3.99×10^{10} $\frac{\mathrm{W}}{\mathrm{cm}^2}$, respectively. Moreover, a pronounced enhancement (up to an order of magnitude for laser-field intensities close to 3.99×10^{10} $\frac{\mathrm{W}}{\mathrm{cm}^2}$) of groups of n-photon detachment rates is observed near the even (i.e., 8 and 10) channel closures. One observes in Fig. 2 four different types of threshold behaviors of the open-channel rates at the detachment thresholds, as predicted by Baz' in Ref. [24]. As noted by Borca *et al.* [17], the most remarkable feature of the ATD spectrum, which they explain as "an interplay of potential- and laser-induced effects," is that the enhancement occurs for n-photon detachment rates on the ATD plateau. In fact, it appears to be most pronounced in the lower-energy part of the rescattering plateau, where the influence of the atomic potential is strongest.

Figure 3 displays a similar intensity dependence of the partial rates, $\Gamma^{(n)}$, for detachment of the F^- ion (averaged over the projections of the angular momentum $l=1$) for channels $7\leqslant n\leqslant 70$ in the region of intensities where, owing to the increasing ponderomotive shift with increasing intensity, the $n=7$, 8, 9, and 10 channels become closed. These closures occur at the laser-field intensities $I=4.69$, 6.97, 9.3, and 11.72×10^{12} $\frac{\mathrm{W}}{\mathrm{cm}^2}$, respectively. Comparing Figs. 2 and 3, one observes that for fixed intensity of the laser field, the ATD partial rates for the s- and p-electron detachment processes show qualitatively different behavior in the plateau region: while both have nearly equal rates for n values on the plateau, for the s-electron initial state the rates form a monotonically decreasing, dense structure as a function of increasing n, whereas in the case of the p-electron initial state the rates cross each other. This indicates a much more pronounced interference in the high-energy part of the ATD spectrum for the p- than for the s-symmetry initial state, which has been noted also in Ref. [41].

The present and previous [17] calculations show that the threshold enhancements appear not in the next available channel, but in channels with much higher energy. For example, at the intensity corresponding to the seven-photon threshold of F^- $\left(I=4.69\times10^{12}\ \frac{\mathrm{W}}{\mathrm{cm}^2}\right)$, the cusp becomes visible only in the $n=14$ channel and extends roughly to the $n=28$ channel. In order to explain this phenomenon, we employ the rescattering model [6,7], which suggests that if a photoelectron whose initial energy is zero returns back to the origin and interacts with or "rescatters" from the core, then its final energy lies in the range between $3.17U_p$ and $10U_p$ [5]. Thus, one can assume that the interchannel coupling is strong when the channel energy difference lies exactly in this range, i.e., the range of energies to which electrons are rescattered. This may be illustrated for the case of the $n=7$ threshold. As noted above, this channel becomes closed when the laser intensity is 4.69×10^{12} $\frac{\mathrm{W}}{\mathrm{cm}^2}$, which corresponds to a ponderomotive energy of $U_p=0.0511$ a.u., so that $3.17U_p/\omega=6.5$ and $10U_p/\omega=20.6$. This means that channels that are strongly coupled to the $n=7$ channel correspond to $14<n<28$, which agrees with the results of our numerical calculations. If one next considers the $n=9$ threshold, the corresponding ponderomotive energy is 0.1034 a.u., which leads to the following range of channels n being strongly coupled with the $n=9$ channel: $22<n<50$. This also agrees with the results of our calculations. Similar con-

siderations apply as well to the H^- spectrum (cf. Fig. 2).

Notice that not all $(n+m)$-photon channels demonstrate the rate enhancement at the closing of the n-photon channel, but only a range of ATD channels on the plateau do. Clearly the atomic potential plays a key role in facilitating interactions between different multiphoton channels. Thus it is mainly electrons that return to the atomic core, i.e., the rescattered electrons, whose initial and final channels undergo interaction. Since ATD plateaus originate from rescattering processes, it is only ATD plateau channels that can therefore become enhanced at the closing of lower-energy multiphoton channels. This contrasts with a Rydberg resonance or light-induced resonance interpretation of the enhancements, which one would expect to enhance the entire ATD spectrum and not just a limited range of ATD channels.

Another notable feature in the enhancements of the ATD spectra revealed by comparison of our numerical results for the hydrogen and fluorine negative ions is that they are qualitatively different. While the enhancements for H^- (having an s outer electron) are pronounced for open channels at the even-channel closures, for F^- (having a p outer electron) the pronounced enhancements manifest themselves when the odd channels are closed. Therefore, our assumption about the s-wave dominance near the threshold made in the previous section is reasonable, i.e., that it is the closure of s-wave channels accessible from the initial state that results in the most pronounced enhancements. On the other hand, the assumption about the two-channel coupling dominance is not very well justified, since there is an entire group of $(n+m)$-photon absorption channels that are strongly coupled to the n-photon channel. Therefore not all $(n+m)$-photon channels grow in magnitude as the intensity increases toward the n-photon threshold, as suggested by Eqs. (35) and (36).

VI. ANGULAR DISTRIBUTIONS

Dramatic changes of few photon angular distributions (ADs) with varying laser intensity near detachment thresholds have been studied both experimentally [47,48] and theoretically [49,50] for the case of H^-. In Ref. [49], the behaviors of angular distributions for electrons detached by two and three elliptically polarized photons were investigated near CCs. The angular distributions for two-photon detachment by linearly polarized light near the corresponding CC were studied experimentally in Refs. [47,48] and investigated theoretically in Ref. [50]. The angular distribution of ATD electrons for F^- [41,43,51] as well as for other halogen negative ions [51] was investigated for fixed laser intensity, and comparisons were made to those for H^- [41,51]. In contrast to these prior works for F^-, the present work investigates the intensity dependence of the ADs of electrons detached from F^- in the vicinity of multiphoton channel closings.

In Figs. 4 and 5, we demonstrate the intensity dependence of the eight- and nine-photon ADs for F^- detachment by a linearly polarized laser field having a frequency $\omega = 0.0253$ a.u. for the cases in which the laser-field intensity approaches the values corresponding to the closing of these particular thresholds. (Note that the detachment rates have been averaged over the projections of the initial-state orbital angular momentum, $l=1$.) For the eight-photon detachment channel near its threshold, the ADs for different intensities are all peaked along the polarization direction of the laser field (i.e., along the horizontal axis in Fig. 4), and no electrons are ejected in the perpendicular direction. A more interesting behavior of the ADs with changing laser-field intensity is observed in Fig. 5. While at lower intensities the ADs for the nine-photon detachment channel near the nine-photon threshold are peaked along the polarization vector of the laser field $\hat{\boldsymbol{\varepsilon}}$, as the intensity of the laser field increases slightly the ADs change dramatically with their maximum pointing perpendicular to the laser-field polarization. In particular, for the intensity $I = 9.21 \times 10^{12} \frac{\mathrm{W}}{\mathrm{cm}^2}$ the emission of the detached

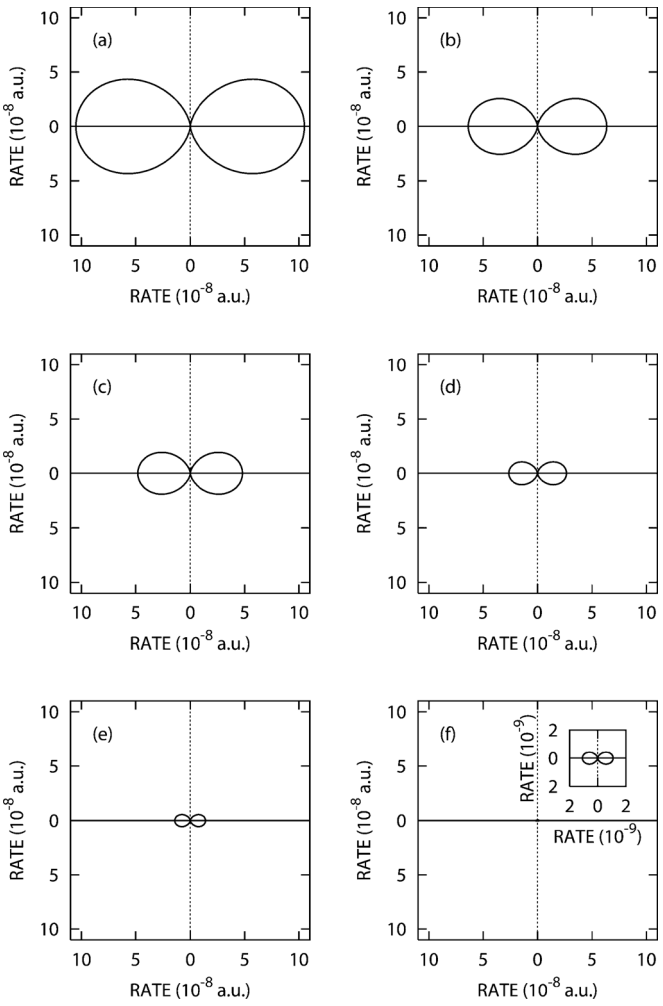

FIG. 4. Angular distributions (ADs) for F^- detachment by eight photons (averaged over the projections of the initial angular momentum, $l=1$) for a linearly polarized laser field of frequency $\omega = 0.0253$ a.u. when the laser-field intensity is varied in the vicinity of the closing of the eight-photon channel, i.e., $I=6.94$, 6.95, 6.954, 6.96, 6.964, and $6.97 \times 10^{12} \frac{\mathrm{W}}{\mathrm{cm}^2}$ (in order from top left to bottom right panels). The ADs for each intensity are peaked along the direction of the laser polarization $\hat{\boldsymbol{\varepsilon}}$, which is marked by the solid horizontal line in each panel; no electrons are observed to be ejected perpendicularly to $\hat{\boldsymbol{\varepsilon}}$.

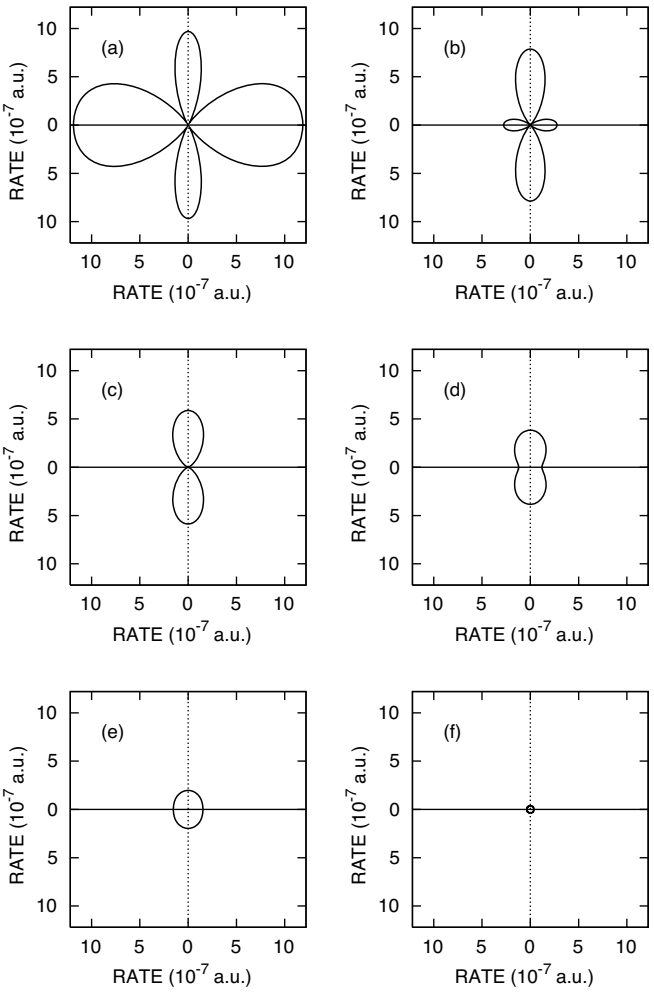

FIG. 5. The same as in Fig. 4 for the nine-photon channel near the closing of the nine-photon channel for six laser-field intensities, $I=8.90$, 9.10, 9.21, 9.26, 9.29, and 9.30×10^{12} $\frac{\mathrm{W}}{\mathrm{cm}^2}$ (from top left to bottom right panels, respectively). The ADs, initially peaked along the laser-field polarization $\hat{\boldsymbol{\varepsilon}}$, for higher intensities become strongly peaked in the perpendicular direction (for $I=9.21\times10^{12}$ $\frac{\mathrm{W}}{\mathrm{cm}^2}$ the probability for electron detachment in the direction of $\hat{\boldsymbol{\varepsilon}}$ is zero), whereas at intensities close to the threshold they become isotropic.

electrons along the laser polarization is zero. For still higher intensities, approaching the threshold for nine-photon detachment, the AD becomes isotropic. Similarly dramatic changes in the shapes of the ADs for other odd multiphoton detachment channels of F^- as a function of laser-field intensity in the vicinity of the channel closings have been found in our calculations, while the more usual or expected ADs found for the eight-photon channel have been found also for other even multiphoton channels. In contrast, we find that the behaviors of the ADs for odd- and even-photon channels for an H^- ion (having initial orbital angular momentum, $l=0$) are reversed. These AD results demonstrate once more the importance of the symmetry of the initial electron state, i.e., whether it is an s or p electron.

In order to explain the peculiar behaviors of the ADs near the thresholds, we employ the Keldysh-like theory developed in Ref. [52]. As shown by Gribakin and Kuchiev [46], at threshold, when the kinetic energy of the detached electron is

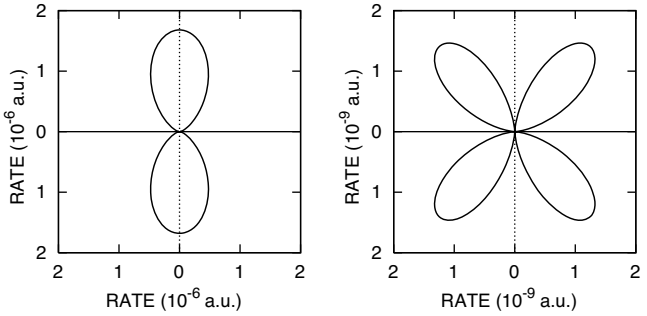

FIG. 6. The ADs for the nine-photon detachment channel of F^- by a laser field of frequency $\omega=0.0253$ a.u. and linear polarization along the horizontal axis, for an intensity $I=9.21\times10^{12}$ $\frac{\mathrm{W}}{\mathrm{cm}^2}$. The left panel corresponds to detachment of an initial state with $(l,m)=(1,0)$, whereas the right panel corresponds to initial states $(l,m)=(1,1)$ or $(1,-1)$. The average of these ADs over the initial-state angular momentum projections is presented in Fig. 5(c).

low compared to its binding energy in the atomic potential, namely $p^2/2 \ll |E_0|$, the n-photon detachment angular distribution from an atomic state of angular momentum l and projection m behaves like [cf. Eq. (42) in Ref. [46]],

$$\frac{d\Gamma^{(n)}}{d\Omega} \sim p\left(\frac{p\sin\theta}{\kappa}\right)^{2|m|} \exp\left[\frac{p^2}{\omega}\left(\frac{\gamma}{\sqrt{1+\gamma^2}} - \sinh^{-1}\gamma\right)\right] \times \exp\left(-\frac{\gamma p^2 \sin^2\theta}{\omega\sqrt{1+\gamma^2}}\right)\left[1+(-1)^{n+l+m} \times \cos\left(\frac{2\kappa p\cos\theta\sqrt{1+\gamma^2}}{\omega\gamma}\right)\right], \tag{38}$$

where $\kappa=\sqrt{-2E_0}$ and $\gamma=\kappa\omega/\mathcal{F}_0$ is the Keldysh parameter. [Note that in this analysis, we are only considering terms that depend on the angle θ (between the electron momentum $\boldsymbol{p}$ and the polarization vector of the laser field $\hat{\boldsymbol{\varepsilon}}$) and on the magnitude of electron momentum, $|\boldsymbol{p}| \equiv p$.] It follows from Eq. (38) that the detachment rate for the state with $m\neq0$ is much smaller than that for $m=0$, owing to the presence of the term $(p\sin\theta/\kappa)^{2|m|}$. This is exactly what one sees in Fig. 6, which shows the angular distributions for the nine-photon detachment channel of the F^- ion by a linearly polarized laser field (with polarization direction marked by the solid horizontal line) having frequency $\omega=0.0253$ a.u. and intensity $I=9.21\times10^{12}$ $\frac{\mathrm{W}}{\mathrm{cm}^2}$, which is very close to that necessary to close the nine-photon channel, i.e., $I=9.3\times10^{12}$ $\frac{\mathrm{W}}{\mathrm{cm}^2}$. The left panel in Fig. 6 corresponds to the initial state with $m=0$, whereas the right panel corresponds to $m=1$ or -1. Note that the detachment rates between these cases differ by three orders of magnitude. A remarkable feature of these ADs is that in each case there is no emission of the detached electrons along the direction of laser polarization. For $m=0$, the AD is peaked in the perpendicular direction. This can also be explained on the basis of Eq. (38). Namely, it follows from the interference term in the last set of square brackets in Eq. (38) that the detachment rates are zero for photoelectrons emitted perpendicularly to the laser field, $\theta=\pi/2$, when $n+l+m$ is odd, and that they are maximal when $n+l+m$ is

even. In the case considered, i.e., the $n=9$ channel for a p-electron ($l=1$) initial state, for $m=0$ we observe an AD that is peaked perpendicularly to the laser field, and for the other values of m the probability of electron photoemission at the angle $\theta=\pi/2$ is zero. As follows also from Eq. (38), for the ejection angle $\theta=0$ there are obviously no detached electrons observed for $m\neq 0$. Finally, we note that since the ADs presented in Figs. 4 and 5 are mainly influenced by the contribution of the $m=0$ initial state, one can describe without loss of generality the ADs near channel-closing thresholds using Eq. (38) for this case. For very small photoelectron kinetic energies near the threshold, one can expand the formula for the differential partial rate (38) for $m=0$ with respect to small p. One finds that $d\Gamma^{(n)}/d\Omega$ is proportional to p for $n+l$ having even values, whereas for $n+l$ odd it is proportional to $p^3\cos^2\theta$, as has been noted in Ref. [48]. This explains the threshold behavior of the ADs demonstrated in Figs. 4 and 5 [(f) panel in each figure].

We note in concluding this section that we have also investigated the intensity dependence of the ADs of ATD plateau electrons in the vicinity of CCs. We have found generally that while the topological shapes of the ADs remain unchanged, both the relative and absolute magnitudes of the different lobes of the ADs may in many cases change, in some instances dramatically. In addition, the results exhibit sensitivity to the initial-state symmetry of the active electron. These results for ADs of plateau electrons will be presented elsewhere.

VII. CONCLUSIONS

Our finite-range model potential results for ATD rates and detached electron angular distributions for the H^- and F^- negative ions show dramatic changes with varying laser-field intensity in the vicinity of multiphoton detachment channel closings. These changes have been interpreted analytically. The results for H^- confirm results obtained within the ZRP model for ATD plateau enhancements [17]. We expect that similar enhancements will occur when the channels are closed by changing the laser frequency, as has been predicted for H^- in [17]. Our results have demonstrated the importance of the initial-state symmetry of the active electron. Depending on the s or p symmetry, very pronounced enhancements of the low- to mid-energy regions of the ATD plateau have been found for intensities in the vicinity of even- or odd-photon detachment channel closings, respectively. Remarkable also is that in our model for F^- detachment, multiphoton resonances between the bound atomic states have turned out *not* to influence the enhancements in the high-order ATD spectrum. We conclude, therefore, that threshold anomalies at channel closings offer a clear and fully satisfactory explanation of resonant-like enhancements of high-energy ATD spectra, and we suspect that the same explanation likely holds also for the high-energy above-threshold ionization of neutral atoms, as observed experimentally for rare gases [8–13].

Variations in the ATD electron ADs with changing laser intensity in the vicinity of channel closings have also been found. These ADs have been shown to be highly sensitive to the initial-state symmetry. Our results are consistent with the predictions of Ref. [46].

Note added in proof. Recently we were informed by N. L. Manakov of calculations for multiphoton detachment of F^- using effective range theory [N. L. Manakov and M. V. Frolov, JETP Lett. **83**, 536 (2006)]. Although carried out for a different laser frequency, those results appear to be consistent with the finite-range potential Floquet-Sturmian results in this paper.

ACKNOWLEDGMENTS

This work was supported in part by the Polish Committee for Scientific Research under Grant No. KBN 1 P03B 006 28 (K.K.), the U.S. National Science Foundation under Grants No. PHY-0354688 (I.I.F.) and No. PHY-0300665 (A.F.S.), and by the University of Nebraska–Lincoln (K.K.).

APPENDIX: NORMALIZATION OF RATES FOR H^- DETACHMENT TREATED IN THE SINGLE-ACTIVE-ELECTRON APPROXIMATION

In calculations of photodetachment of negative ions involving the use of a model potential within the SAE approach, there is apparently much confusion regarding the proper normalization of the final result. We discuss this problem in detail here for the illustrative case of the H^- ion, which has been treated in different ways by many authors. At the end of this appendix, we note our generalization for the case of the F^- ion.

Many authors (see, e.g., [34,37,46,53,54]) claim that since there are two equivalent electrons in the $1s^2$ subshell, the final result for the photodetachment cross sections for H^- should be multiplied by a factor of 2. At the same time, some of them (e.g., [46,53,54]) use the zero-range potential model to describe the initial state

$$\psi_1(r) = B\frac{e^{-\kappa r}}{r}, \tag{A1}$$

where $\kappa=\sqrt{-2E_1}$, and fail to use the proper normalization coefficient B. In the pure ZRP model, $B_0=\sqrt{\kappa/2\pi}$. However, it has been known since the work of Bethe and Longmire [55] that in order to account for the finite range of the e-H interaction, one should use a different normalization constant, $B=1.629B_0$ (see, for instance, Ref. [56]). This happens because the ZRP model overestimates the electron probability density near the nucleus. Laughlin and Chu [57] noted that Geltman's calculations [54] fail to use the proper value of B, but multiply the cross sections by a factor 2 because of the two electrons in the $1s^2$ subshell. (The same procedure was adopted by Becker *et al.* [53].) As a result, Geltman's cross sections are too small by about a factor of $(1.6290)^2/2=1.327$ as compared to the results of Chu and coauthors [45,57–59]. Note that Chu and coauthors do not have the extra factor of 2; they also use a more sophisticated potential for describing the e-H interaction. Thus the ratio of their cross sections to those calculated by Geltman [54] is not exactly 1.327, but varies with energy.

Gribakin and Kuchiev [46] do not use the zero-range potential model explicitly, but they introduce the asymptotic coefficient in the initial wave function ψ_1, $A=B\sqrt{4\pi}$. With their choice of $A=0.75$, we obtain $B=0.212$, which is close to $B_0=0.194$, while the correct value, according to Refs. [56,60], should be $B=0.315$. Like Geltman, Gribakin and Kuchiev use the factor 2 in their final result, so that their results are in agreement with those of Chu *et al.*

Whereas there is no doubt that the proper normalization constant, $B=0.315$, should be used in photodetachment calculations, the situation regarding the factor of 2 in the cross section is not quite clear. Let us discuss this issue in more detail in connection with the one-photon detachment process.

In restricted Hartree-Fock calculations, the two equivalent electrons in the $1s^2$ subshell are described by the same orbital, and the two-electron wave function for the initial state can be written in the form

$$\Psi_i(r_1,r_2)=\psi_1(r_1)\psi_1(r_2). \tag{A2}$$

The final-state wave function in the independent-electron approximation is

$$\Psi_f(\boldsymbol{r}_1,\boldsymbol{r}_2)=\frac{1}{\sqrt{2}}[\psi_{1s}(r_1)\phi_{\boldsymbol{k}}(\boldsymbol{r}_2)+\psi_{1s}(r_2)\phi_{\boldsymbol{k}}(\boldsymbol{r}_1)], \tag{A3}$$

where $\psi_{1s}(r)$ is the $1s$ hydrogenic orbital, and $\phi_{\boldsymbol{k}}(\boldsymbol{r})$ is a properly normalized plane wave that corresponds to the final-electron wave vector $\boldsymbol{k}$. The dipole matrix element (for simplicity, we consider only one Cartesian component of the dipole operator $\boldsymbol{D}_1+\boldsymbol{D}_2$),

$$M_{\boldsymbol{k}}=\langle\Psi_f|D_1+D_2|\Psi_i\rangle, \tag{A4}$$

calculated with those functions, is

$$M_{\boldsymbol{k}}=M_{\boldsymbol{k}}^{(1)}\sqrt{2}\langle\psi_{1s}|\psi_1\rangle, \tag{A5}$$

where $M_{\boldsymbol{k}}^{(1)}$ is the one-electron matrix element. Thus the one-photon detachment cross section is

$$\sigma=2\sigma^{(1)}|\langle\psi_{1s}|\psi_1\rangle|^2. \tag{A6}$$

If we assume here that the overlap integral $\langle\psi_{1s}|\psi_1\rangle=1$, then we obtain $\sigma=2\sigma^{(1)}$. However, this assumption is not justified. The form of the initial-state orbital, Eq. (A1), although good for calculation of the photodetachment matrix element, does not give a reliable result for the overlap. In particular, if we use $B=0.315$, the overlap is 1.465, which is physically meaningless. On the other hand, for $B=B_0=0.194$, the value of the overlap is 0.882, which suggests that the one-electron cross section should be multiplied not by a factor of 2, but by a factor 1.55.

To investigate this matter in more detail, we plot in Fig. 7 the three H^- radial wave functions $u_1(r)$ $[\psi_1(r)=u_1(r)/(r\sqrt{4\pi})]$ calculated, respectively, with the use of the Yukawa potential of Shakeshaft *et al.* [34] employed in the present work, the potential of Laughlin and Chu [57], and the zero-range potential [56]. In the latter case, we use $B=0.315$ for the normalization constant. We see that the accurate potential of Laughlin and Chu, which includes the long-range polarization interaction, leads to the proper asymptotic behavior of the wave function. In particular, the asymptotic

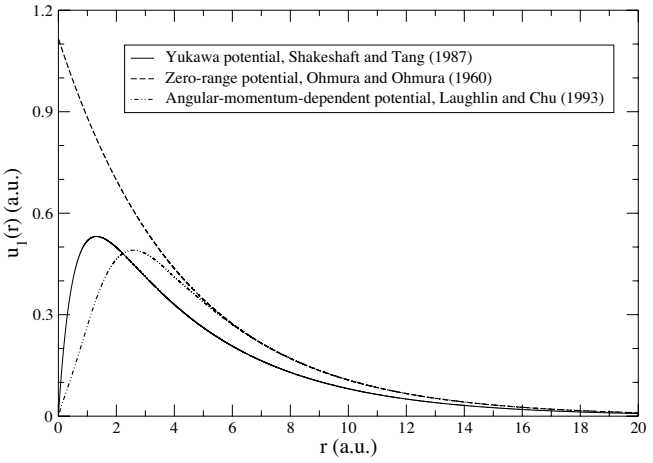

FIG. 7. Comparison of the radial electron wave functions for three different model potentials [34,56,57], as noted in the figure, describing H^- within the SAE approximation.

coefficient B is equal to the proper value $B=0.315$ within 1% accuracy. At the same time, the function obtained from the Yukawa potential has a higher probability density at smaller distances, which leads to $B_{\text{Yukawa}}/B=0.760$. The values of the overlap integral are 0.882 and 0.691 for the Yukawa and Laughlin and Chu potentials, respectively. This leads, according to Eq. (A6), to $\sigma=1.55\sigma^{(1)}$ for the Yukawa potential and $\sigma=0.955\sigma^{(1)}$ for the Laughlin and Chu potential. It is evident now that the agreement with Laughlin and Chu, which Shakeshaft *et al.* obtain after introducing an extra factor of 2 in their cross section, has nothing to do with the two-electron character of the problem, but rather with the normalization of $\psi_1(r)$.

There is actually a more serious problem with using the initial wave function in the form (A2). It is well known that this form does not result in a positive electron affinity for hydrogen H. Indeed, the best variational value of κ, $\kappa=0.6875$, gives -0.473 a.u. for the binding energy of H^-, which is higher than the energy of the neutral hydrogen atom. One can try to improve the situation by introducing the unrestricted Hartree-Fock wave function containing two different orbitals for $1s$ electrons, i.e.,

$$\Psi_i(r_1,r_2)=\frac{1}{\sqrt{2}}[\psi_1(r_1)\psi_2(r_2)+\psi_1(r_2)\psi_2(r_1)]. \tag{A7}$$

By choosing

$$\psi_1(r)=c_1e^{-\alpha r},\quad \psi_2(r)=c_2e^{-\beta r}, \tag{A8}$$

one can obtain a total energy of H^- below -0.5 a.u. In particular, choosing $\alpha=1$, $\beta=0.25$ one gets $E=-0.5122$ a.u., which corresponds to an electron affinity of 0.33 eV. Of course, for more accurate values of the affinity, a function with many variational parameters should be used. If one calculates the photodetachment matrix element using the function (A7), one obtains

$$M_{\boldsymbol{k}} = M^{(1)}_{\boldsymbol{k},1}\langle\psi_{1s}|\psi_2\rangle + M^{(1)}_{\boldsymbol{k},2}\langle\psi_{1s}|\psi_1\rangle, \tag{A9}$$

where $M^{(1)}_{\boldsymbol{k},i}$ is the one-electron matrix element corresponding to the removal of the electron occupying the orbital i.

It is clear now that at energies close to the photodetachment threshold, the process of detachment of the electron from the orbital with lower binding energy (say, the orbital ψ_2) will dominate, so there is no justification for multiplying the one-electron cross section by the factor 2. However, for higher energies the detachment of the electron from the orbital ψ_1 becomes important. In order to investigate the competition between these two processes, we present the matrix element $M_{\boldsymbol{k}}$ for the case of an initial-state wave function having the form given in Eqs. (A7) and (A8). Up to an overall numerical factor (which is not essential for our purposes here), we obtain that

$$M_{\boldsymbol{k}} \sim \cos\,\theta_{\boldsymbol{k}}(\alpha\beta)^{3/2}\left[\frac{1}{(\alpha^2+k^2)^2(1+\beta)^3} + \frac{1}{(\beta^2+k^2)^2(1+\alpha)^3}\right], \tag{A10}$$

where $\theta_{\boldsymbol{k}}$ is the angle between the wave vector $\boldsymbol{k}$ and the photon polarization vector $\hat{\boldsymbol{\varepsilon}}$. At the threshold, $k=0$, the ratio of the first to the second term is $0.512/32=0.016$. This means that the one-electron expression for the cross section is reasonably accurate, and the factor of 2 in the final result is not justified. However, with the growth of k^2 the ratio increases dramatically and reaches 4.096 at $k \gg \alpha$. This has a clear physical meaning: at high energies, the process of removal of the electron from the inner orbital becomes dominant. However, the enhancement factor (as compared to the ZRP model) becomes much greater than 2.

In summary, the one-electron model for H^- detachment can be used only at relatively low energies when the process of electron removal from the orbital with higher binding energy is not important. In particular, the model can be used in studies of threshold effects in multiphoton detachment, which is the main purpose of the present paper. The absolute values of our rates are not accurate, however, for two reasons: first, because of the normalization factor in the one-electron wave function, and second because of the importance of two-electron effects at higher energies. However, there is absolutely no justification for the extra factor of 2 in the final cross sections. Also, on the basis of similar arguments, one can draw the conclusion that there is no need to multiply the results for F^-, obtained within the analogous single-active-electron model, by a factor of 6 owing to the degeneracy of the initial p state.

[1] P. Agostini, F. Fabre, G. Mainfray, G. Petite, and N. K. Rahman, Phys. Rev. Lett. **42**, 1127 (1979).
[2] L. F. DiMauro and P. Agostini, Adv. At., Mol., Opt. Phys. **35**, 79 (1995).
[3] M. Protopapas, C. H. Keitel, and P. L. Knight, Rep. Prog. Phys. **60**, 389 (1997).
[4] N. B. Delone and V. P. Krainov, Phys. Usp. **41**, 469 (1998).
[5] W. Becker, F. Grasbon, R. Kopold, D. B. Milošević, G. G. Paulus, and H. Walther, Adv. At., Mol., Opt. Phys. **48**, 35 (2002).
[6] K. J. Schafer, B. Yang, L. F. DiMauro, and K. C. Kulander, Phys. Rev. Lett. **70**, 1599 (1993).
[7] P. B. Corkum, Phys. Rev. Lett. **71**, 1994 (1993).
[8] P. Hansch, M. A. Walker, and L. D. Van Woerkom, Phys. Rev. A **55**, R2535 (1997).
[9] M. P. Hertlein, P. H. Bucksbaum, and H. G. Muller, J. Phys. B **30**, L197 (1997).
[10] M. J. Nandor, M. A. Walker, L. D. Van Woerkom, and H. G. Muller, Phys. Rev. A **60**, R1771 (1999).
[11] E. Cormier, D. Garzella, P. Breger, P. Agostini, G. Chériaux, and C. Leblanc, J. Phys. B **34**, L9 (2000).
[12] G. G. Paulus, F. Grasbon, H. Walther, R. Kopold, and W. Becker, Phys. Rev. A **64**, 021401(R) (2001).
[13] F. Grasbon, G. G. Paulus, H. Walther, P. Villoresi, G. Sansone, S. Stagira, M. Nisoli, and S. De Silvestri, Phys. Rev. Lett. **91**, 173003 (2003).
[14] H. G. Muller and F. C. Kooiman, Phys. Rev. Lett. **81**, 1207 (1998).
[15] H. G. Muller, Phys. Rev. A **60**, 1341 (1999).
[16] R. Kopold, W. Becker, M. Kleber, and G. G. Paulus, J. Phys. B **35**, 217 (2002).
[17] B. Borca, M. V. Frolov, N. L. Manakov, and A. F. Starace, Phys. Rev. Lett. **88**, 193001 (2002).
[18] S. V. Popruzhenko, Ph. A. Korneev, S. P. Goreslavski, and W. Becker, Phys. Rev. Lett. **89**, 023001 (2002).
[19] J. Wassaf, V. Véniard, R. Taïeb, and A. Maquet, Phys. Rev. Lett. **90**, 013003 (2003).
[20] J. Wassaf, V. Véniard, R. Taïeb, and A. Maquet, Phys. Rev. A **67**, 053405 (2003).
[21] K. C. Kulander, K. J. Schafer, and J. L. Krause, in *Atoms in Intense Laser Fields*, edited by M. Gavrila (Academic, Boston, 1992), p. 247.
[22] R. Bhatt, B. Piraux, and K. Burnett, Phys. Rev. A **37**, 98 (1988).
[23] R. M. Potvliege, Phys. Rev. A **62**, 013403 (2000).
[24] A. I. Baz', Sov. Phys. JETP **6**, 709 (1958).
[25] A. M. Lane and R. G. Thomas, Rev. Mod. Phys. **30**, 257 (1958).
[26] M. H. Ross and G. L. Shaw, Ann. Phys. (N.Y.) **13**, 147 (1961).
[27] M. Gailitis, Sov. Phys. JETP **17**, 1328 (1963).
[28] A. I. Baz', Ya. B. Zel'dovich, and A. M. Perelomov, *Scattering, Reactions and Decays in Nonrelativistic Quantum Mechanics* (Nauka, Moscow, 1971), Sec. IX.
[29] L. D. Landau and E. M. Lifshitz, *Quantum Mechanics* (Pergamon, Oxford, 1977), Sec. 417.
[30] K. Krajewska, I. I. Fabrikant, and A. F. Starace, Bull. Am. Phys. Soc. **51**, 119 (2006).
[31] R. M. Potvliege and R. Shakeshaft, in *Atoms in Intense Laser Fields*, edited by M. Gavrila (Academic, Boston, 1992), p. 373.

[32] R. M. Potvliege, Comput. Phys. Commun. **114**, 42 (1998).
[33] I. S. Gradshteyn and I. M. Ryzhik, *Table of Integrals, Series and Products* (Academic, San Diego, 1980).
[34] R. Shakeshaft and X. Tang, Phys. Rev. A **36**, 3193 (1987).
[35] R. M. Potvliege and R. Shakeshaft, Phys. Rev. A **38**, 4597 (1988).
[36] R. M. Potvliege and R. Shakeshaft, Phys. Rev. A **38**, 6190 (1988).
[37] M. Dörr, R. M. Potvliege, D. Proulx, and R. Shakeshaft, Phys. Rev. A **42**, 4138 (1990).
[38] K. R. Lykke, K. K. Murray, and W. C. Lineberger, Phys. Rev. A **43**, 6104 (1991).
[39] C. Blondel, P. Cacciani, C. Delsart, and R. Trainham, Phys. Rev. A **40**, 3698 (1989).
[40] I. Yu. Kiyan and H. Helm, Phys. Rev. Lett. **90**, 183001 (2003).
[41] M. V. Frolov, N. L. Manakov, E. A. Pronin, and A. F. Starace, Phys. Rev. Lett. **91**, 053003 (2003).
[42] D. B. Milošević, A. Gazibegović-Busuladžić, and W. Becker, Phys. Rev. A **68**, 050702(R) (2003).
[43] M. V. Frolov, N. L. Manakov, E. A. Pronin, and A. F. Starace, J. Phys. B **36**, L419 (2003).
[44] P. G. Burke, P. Francken, and C. J. Joachin, J. Phys. B **24**, 761 (1991).
[45] D. A. Telnov and S.-I. Chu, J. Phys. B **37**, 1489 (2004).
[46] G. F. Gribakin and M. Yu. Kuchiev, Phys. Rev. A **55**, 3760 (1997).
[47] R. Reichle, H. Helm, and I. Yu. Kiyan, Phys. Rev. Lett. **87**, 243001 (2001).
[48] R. Reichle, I. Yu. Kiyan, and H. Helm, J. Mod. Opt. **50**, 461 (2003).
[49] B. Borca, M. V. Frolov, N. L. Manakov, and A. F. Starace, Phys. Rev. Lett. **87**, 133001 (2001).
[50] D. A. Telnov and Shih-I Chu, Phys. Rev. A **66**, 063409 (2002).
[51] A. Gazibegović-Busuladžić, D. B. Milošević, and W. Becker, Phys. Rev. A **70**, 053403 (2004).
[52] A. M. Perelomov, V. S. Popov, and M. V. Terent'ev, Sov. Phys. JETP **23**, 924 (1966).
[53] W. Becker, S. Long, and J. K. McIver, Phys. Rev. A **42**, 4416 (1990).
[54] S. Geltman, Phys. Rev. A **43**, 4930 (1991).
[55] H. A. Bethe and C. Longmire, Phys. Rev. **77**, 647 (1950).
[56] T. Ohmura and H. Ohmura, Phys. Rev. **118**, 154 (1960).
[57] C. Laughlin and Shih-I Chu, Phys. Rev. A **48**, 4654 (1993).
[58] J. Wang, Shih-I Chu, and C. Laughlin, Phys. Rev. A **50**, 3208 (1994).
[59] D. A. Telnov and Shih-I Chu, Phys. Rev. A **50**, 4099 (1994).
[60] Yu. N. Demkov and V. N. Ostrovsky, *Zero-Range Potentials and Their Applications in Atomic Physics* (Plenum, New York, 1988).